CL2F: Close-Loop Communication and Localization Framework for High-Mobility UAV Swarm Networks in Partial GNSS-Denied Environments

Jingpeng Li[†], Yi Zhang[†‡*], Yinchao Chen[†], and Hanni Yu[†]

[†]Department of Information and Communication Engineering, School of Informatics, Xiamen University, China
[‡]Key Laboratory of Multimedia Trusted Perception and Efficient Computing, Ministry of Education of China, Xiamen University, China
[*] Corresponding Author: yizhang@xmu.edu.cn

***Abstract*—Unmanned aerial vehicle (UAV) swarm networks' highly dynamic topology causes unstable links and routing oscillations during collaborative flight missions, while poor Global Navigation Satellite System (GNSS) signals in denied environments worsen swarm coordination. This paper proposes a close-loop communication and localization framework (CL2F) for high-mobility UAV swarms in partial GNSS-denied environments. It tightly co-designs a factor graph-based cooperative localization approach, a location-aware routing mechanism, and a Deep Deterministic Policy Gradient (DDPG)-based adaptive HELLO interval algorithm to iteratively quantify localization reliability and dynamically adjust communication strategies. Evaluations on a co-simulation platform show the AI-driven framework achieves multi-objective balance among communication overhead, localization accuracy, and network responsiveness under dynamic topology disruptions and signal interference.**

***Index Terms*—UAV swarm network, routing protocol, cooperative localization, deep reinforcement learning.**

I. Introduction

The rapid growth of *unmanned aerial vehicles (UAVs)* has transformed border surveillance, disaster response, and environmental monitoring due to their agility, cost-effectiveness, and sensor-carrying capabilities [1, 2]. UAV swarms need precise positioning and robust inter-UAV communication for collaborative tasks, but face severe signal degradation in *Global Navigation Satellite System (GNSS)*-denied environments (e.g., urban canyons, forests), causing localization failures and disrupted communication [3, 4].

On one hand, conventional routing protocols for stable terrestrial networks fail to adapt to dynamic UAV topologies (high mobility, intermittent connectivity). *Position-based routing protocols* can mitigate topology maintenance overhead via geographic info for path selection. For example, an enhanced greedy perimeter stateless routing (GPSR) with two-hop awareness/reinforcement learning [5] is proposed to adapt to dynamic topologies and an optimized forwarding strategy using a distance metric integrating channel characteristics [6] is introduced to achieve superior packet delivery rates and throughput. On the other hand, GNSS-dependent localization suffers accuracy loss/outages from obstructions/interference. *Cooperative localization* (e.g., ranging-based) offers alternatives, with factor graph (FG)-based methods, i.e., a distributed FG with adaptive diffusion [7] and a weighted FG using Fisher info/Kullback-Leibler divergence to boost reliability [8].

Moreover, recent advances focus on deep communication-localization coupling to address inefficient resource utilization and compromised mission reliability. For example, a two-stage indoor localization framework combining sparse Bayesian learning with support vector machine (SVM) spatial classification is proposed, which demonstrates robustness in complex electromagnetic conditions [9]. A model predictive control framework is provided to balance solar energy harvesting, communication services, and autonomous localization for UAVs [10]. To further advance this research, an air-ground fused localization architecture is devised to optimize position-power relationships through dynamically deployed UAV line-of-sight links [11].

Based on the above discussions, we know that positioning data enables intelligent routing (e.g., topology-aware path selection), while reliable communication supports collaborative localization (e.g., sharing ranging measurements). However, existing integrated frameworks neglect real-time localization reliability assessment and adaptive resource allocation, which may misguide routing and reduce cooperative localization accuracy with unstable links. This paper proposes a close-loop communication and localization framework (CL2F) for high-mobility UAV swarms in partial GNSS-denied environments. Two modules are co-designed: a localization module using weighted factor graph optimization to distributedly estimate UAV geographic information, and a communication module with a location-aware routing mechanism (based on estimated positions) and a DDPG-driven algorithm to adaptively adjust HELLO intervals for timely topology updates. Evaluated on an NS-3/NS3-Gym/GTSAM co-simulation platform, CL2F achieves multi-objective balance among communication overhead, localization accuracy, and network responsiveness.

II. System Model

As illustrated in Fig. 1, we consider a high-mobility UAV swarm composed of m autonomous mobile UAVs equipped

This work was supported by the National Natural Science Foundation of China under Grants 62401485. (Corresponding author: Yi Zhang. Email: yizhang@xmu.edu.cn)

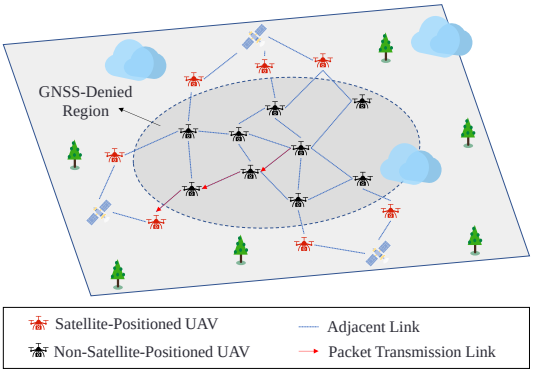

Fig. 1. UAV swarm networks in partial GNSS-denied environments.

with GNSS receivers, denoted by $U = \{u_1, u_2, ..., u_m\}$. Each UAV u_i is characterized by its three-dimensional position $X_i(t) = (x_i(t), y_i(t), z_i(t))$ and velocity vector $V_i(t) = (v_{x,i}(t), v_{y,i}(t), v_{z,i}(t))$ at time slot t. Specifically, we assume that the majority of UAVs (highlighted in black) struck in a **GNSS-denied region** (highlighted in gray) and only those UAVs outside the region (highlighted in red) can receive GNSS positioning signals and therefore have satellite positioning capabilities. To ensure the regular flight missions, the UAV swarm forms a self-organizing wireless network and perform cooperative localization to overcome the partial GNSS-denied environments.

A. UAV Mobility Model

The UAV dynamics follow a Gaussian-Markov mobility model formulated through the temporally correlated velocity update equation:

$$V_i(t+1) = \alpha V_i(t) + (1-\alpha)\mu_v + \sigma_v \sqrt{1-\alpha^2} W_i(t), \quad (1)$$

where $\alpha \in [0,1]$ denotes the memory factor governing velocity persistence, μ_v represents the mean velocity vector, σ_v specifies the standard deviation of velocity perturbations, and $W_i(t) \sim \mathcal{N}(0,1)$ indicates standard normal Gaussian noise. Positional updates adhere to classical kinematic equations by

$$X_i(t+1) = X_i(t) + V_i(t)\Delta t, \quad (2)$$

where Δt represents the discrete time interval.

B. Partial GNSS-Denied Model

Let $X_i = [x_i, y_i, z_i]$ represent the state vector of UAV i. For satellite-positioned UAV j, the pseudorange observation $\rho_{j,G}$ from GNSS satellites satisfies

$$\rho_{j,G} = \sqrt{(x_j - x_G)^2 + (y_j - y_G)^2 + (z_j - z_G)^2} + \varepsilon_{j,G}, \quad (3)$$

where $\rho_{j,G}$ denotes the pseudorange measurement, $[x_G, y_G, z_G]$ is the corresponding UAV position obtained by GNSS positioning signals, and $\varepsilon_{j,G} \sim \mathcal{N}(0, \sigma_G^2)$ represents zero-mean Gaussian observation noise.

Additionally, relative distance observations between UAVs are modeled through

$$z_{i,j} = \sqrt{(x_i - x_j)^2 + (y_i - y_j)^2 + (z_i - z_j)^2} + \varepsilon_{i,j}, \quad (4)$$

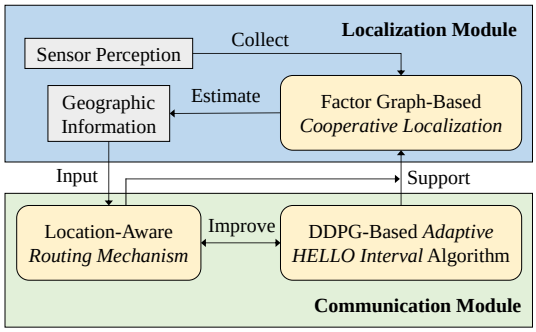

Fig. 2. The proposed close-loop communication and localization framework.

where $z_{i,j}$ denotes the inter-UAV distance measurement with $\varepsilon_{i,j} \sim \mathcal{N}(0, \sigma_d^2)$ representing ranging noise.

C. Topology Awareness Model

To activate dynamic topology awareness, UAVs periodically broadcast HELLO packets containing operational parameters including IP addresses, positional vectors $X_i(t)$, and velocity vectors $V_i(t)$. Through the packet reception and parsing, each UAV can dynamically maintain its neighbor list $n_i(t) = \{u_j \in U \mid z_{i,j}(t) \leq R_c\}$, where $z_{i,j}(t) = \|X_i(t) - X_j(t)\|$ quantifies the Euclidean distance between UAVs u_i and u_j.

The communication range threshold R_c serves as an optimization parameter to ensure network connectivity while eliminating those distant nodes beyond reliable communication distances, thereby maintaining topological stability.

III. Close-Loop Communication and Localization Framework

To address network topology dynamics and communication resource contention of high-mobility UAV swarms in partial GNSS-denied environments, we propose a *close-loop communication and localization framework (CL2F)*. It synergistically integrates communication and localization via a close-loop architecture (environmental perception, decision control, performance feedback), as shown in Fig. 2. The localization module uses distributed cooperative localization to estimate UAV geographic information from sensors. The communication module includes a routing mechanism (optimizing decisions with real-time geographic info) and an adaptive HELLO interval algorithm (adjusting intervals based on topology updates and localization performance). CL2F achieves multi-objective balance among communication overhead, localization accuracy, and network responsiveness.

A. Factor Graph-Based Cooperative Localization

Since each UAV relies on a cooperative approach to achieve high-precision localization in partial GNSS-denied environments, we proposed a factor graph-based cooperative localization algorithm. Each UAV maintains a local factor graph consisting of itself and its neighboring nodes. In this way, the state estimation of the whole UAV swarm can be further modeled as a factor graph, which comprises multiple variable nodes and factor nodes. The variable nodes represent the state of a

UAV and the factor nodes encode the constraint relationships between sensor measurements and physical models, that is, the distance factor f_{dist} and the IMU factor f_{IMU}. Specifically, X_i and X_j are two variable nodes connecting via a range-based factor f_{dist}, which establishes relative positional constraints:

$$f_{\text{dist}}(X_i^{(t)}, X_j^{(t)}) = \exp\left(-\frac{1}{2}\left\|h_{\text{dist}}(X_i^{(t)}, X_j^{(t)}) - z_{ij}^{(t)}\right\|_{R_d}^2\right), \tag{5}$$

where $h_{\text{dist}}(X_i^{(t)}, X_j^{(t)}) = \left\|X_i^{(t)} - X_j^{(t)}\right\|$ represents the Euclidean distance between UAV i and UAV j.

The temporal continuity constraint is provided by the IMU sensor. Let $X_i^{(t-1)}$ and $X_i^{(t)}$ denote the UAV state variables at two consecutive time steps. These states are linked via the IMU factor f_{IMU} expressed by

$$f_{\text{IMU}}(\hat{X}^{(t)}, X^{(t-1)}) = \exp\left(-\frac{1}{2}\left\|h_{\text{IMU}}(X^{(t-1)}) - \hat{X}^{(t)}\right\|_{Q_k}^2\right), \tag{6}$$

where $h_{\text{IMU}}(X^{(t-1)})$ predicts the state from time $t-1$ to t using the IMU motion model.

To improve the localization accuracy and reduce the computational complexity of the distributed factor graph-based approach, a more concise and effective local factor graph is constructed by selectively incorporating neighboring nodes. The credibility T_i of node i is defined as its number of credible neighbors d_i. A node i is considered credible if and only if

$$T_i = d_i \geq \tau, \tag{7}$$

where τ is the credibility threshold. Then, the most credible factor nodes are selected for optimization. The state estimation is achieved by minimizing the following multi-source fusion objective function:

$$\begin{aligned}\hat{\mathbf{X}} = \arg\min_{\mathbf{X}} &\sum_{i=1}^{M}\sum_{j=1}^{n(i)}\left\|\omega_{ij}\left(\|X_i^{(t)} - X_j^{(t)}\| - z_{ij}^{(t)}\right)\right\|_{\mathbf{R}_D}^2 \\ &+ \sum_{i=1}^{M}\left\|h_{\text{IMU}}(X_i^{(t-1)}) - X_i^{(t)}\right\|_{\mathbf{Q}_k}^2,\end{aligned} \tag{8}$$

where $\|\cdot\|_{R_d}^2$ and $\|\cdot\|_{Q_k}^2$ represent weighted norms with weighting matrices R_d and Q_k, respectively. The ω_{ij} denotes a weighting factor defined as

$$\omega_{ij} = \frac{d_j}{\sum_{k\in n^*(i)} d_k}, \tag{9}$$

where $n^*(i)$ is the set of credible neighbors of UAV i, and d_j is the degree of neighbor node j. The weight ω_{ij} reflects the relative importance of neighbor j in the local factor graph of node i.

The factor graph employs a message-passing algorithm for information exchange and updates. Each variable node propagates its state information to connected factor nodes, which then compute new constraints based on observations and models, feeding them back to the relevant variable nodes. Through iterative optimization, the states of variable nodes are progressively adjusted to satisfy all constraints, ultimately achieving a global/near optimal state estimation.

B. Location-Aware Routing Mechanism

Furthermore, in scenarios where data packets need to be transmitted, a geographic routing protocol is adopted. Each UAV selects the next-hop relay node by computing a neighbor utility function based on its neighbor table. The routing decision directly relies on real-time positional information provided by the localization module. The neighbor utility function is defined as

$$\begin{aligned}U_{C,i}(t) =& w_{\text{LET}} \cdot f_{\text{LET}}(X_C(t), X_i(t)) \\ &+ w_d \cdot LCS_i(t) \cdot f_d(z_{i,D}(t)) \\ &+ w_\theta \cdot f_\theta(X_C, X_i),\end{aligned} \tag{10}$$

which consists of three key components:

1) Link Expiration Time (LET): This component evaluates link stability by analyzing the relative motion between UAVs. Considering the kinematic states of the current node C and neighbor node i, we first establish a 3D relative motion model.

Let $(a, b, c) = (x_C - x_i, y_C - y_i, z_C - z_i)$ denote the relative displacement along three axes and (e, f, g) represent the relative velocity components as follows:

$$e = v_C \cos\theta_C \cos\phi_C - v_i \cos\theta_i \cos\phi_i, \tag{11}$$

$$f = v_C \sin\theta_C \cos\phi_C - v_i \sin\theta_i \cos\phi_i, \tag{12}$$

$$g = v_C \sin\phi_C - v_i \sin\phi_i, \tag{13}$$

where v is the velocity, θ and ϕ are the azimuth and elevation angles, respectively. The Euclidean distance between nodes evolves with time t can be calculated by

$$\begin{aligned}d(t) &= \sqrt{(a+et)^2 + (b+ft)^2 + (c+gt)^2} \\ &= \sqrt{kt^2 + lt + m + R_c^2}.\end{aligned} \tag{14}$$

Here, $k = e^2 + f^2 + g^2$ reflects relative speed magnitude, $l = 2(ae+bf+cg)$ characterizes position-velocity correlation, and $m = a^2+b^2+c^2-R_c^2$ relates initial distance to communication radius R_c. The link breaks when $d(t) = R_c$, yielding the link expiration time as

$$L = \frac{-l + \sqrt{l^2 - 4km}}{2k}. \tag{15}$$

An exponential mapping converts L to a normalized stability metric $f_{\text{LET}} \in (0, 1)$:

$$f_{\text{LET}} = 1 - e^L. \tag{16}$$

2) Neighbor Distance: This component quantifies proximity between neighbor i and destination D:

$$f_d(z_{i,D}(t)) = \min(z_{\min(t)}/z_{i,D}(t), 1), \tag{17}$$

where $z_{i,D}$ is the Euclidean distance between neighbor i and destination D, and $z_{\min} = \min\{z_{j,D}(t) \mid j \in n_C(t)\}$ is the minimum distance among current candidates $n_C(t)$.

To tackle localization accuracy variations, we further introduce a Localization Confidence Score (LCS) for the post-

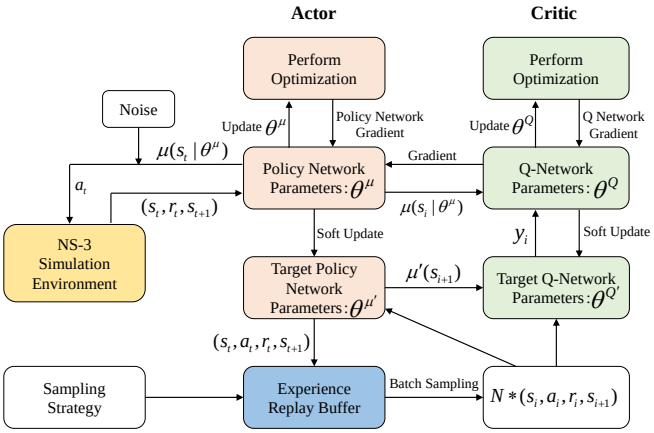

Fig. 3. Structure of DDPG-based adaptive HELLO interval algorithm.

localization of each UAV, that is,

$$LCS_i = \frac{1}{n^*(i)} \sum_{j \in n^*(i)} \omega_{ij} \cdot \exp\left(-\frac{|\|X_i - X_j\| - z_{ij}|^2}{2\sigma_{\text{th}}^2} \right), \tag{18}$$

where $n^*(i)$ is the set of credible neighbors, ω_{ij} is a weight, and σ_{th} is the error tolerance threshold. It should be noted that the routing weights can dynamically adjusted by introducing the LCS factor. When localization errors increase, the routing decision based on Eq. (10) will tend to f_{LET} and f_θ and therefore the accuracy loss through link quality and geometric consistency could be compensated.

3) Directional Consistency: This component exploits geometric vector relationships and can be calculated by

$$f_\theta(z_{C,i}(t), z_{C,D}(t)) = \frac{z_{C,D}^2(t) + z_{C,i}^2(t) - z_{i,D}^2(t)}{2 z_{C,i}(t) z_{C,D}(t)}, \tag{19}$$

where $z_{C,i}(t)$ and $z_{C,D}(t)$ are Euclidean distances from node C to neighbor i and destination D, respectively.

C. DDPG-Based Adaptive HELLO Interval Algorithm

The high mobility of UAV swarms increases the difficulty of real-time routing topology updates. That is, a higher HELLO frequency ensures timely topology updates but raises communication overhead and energy consumption, while a lower frequency saves resources but leads to outdated topology information and degraded routing performance. Additionally, HELLO frequency significantly affects the convergence speed of factor graph-based cooperative localization and computational resource utilization. Therefore, we leverage DDPG's advantage in continuous action space control and propose a DDPG-based adaptive HELLO interval algorithm to dynamically optimize communication and localization performance.

The proposed algorithm comprises three core components:

- **State Space:** The state space $\mathcal{S}$ characterizes network dynamics, with state vector $\mathbf{s}_t \in \mathcal{S}$ defined as

$$\mathbf{s}_t = [n_i(t), v_i(t), f_T, \rho_c(t), S(t), \mathbb{E}[\Delta n_i(t)], LCS_i(t)], \tag{20}$$

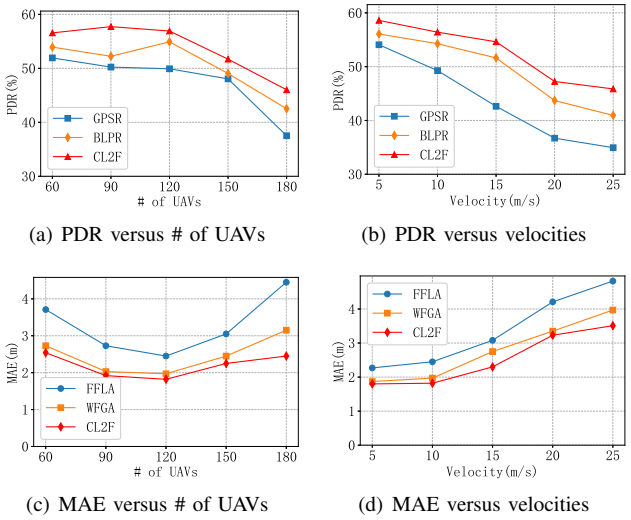

Fig. 4. Evaluation results based on the co-simulation platform.

where $n_i(t)$ is neighbor count, $v_i(t)$ node velocity, f_T HELLO frequency, $\rho_c(t)$ channel busy ratio (measured via carrier sensing), $S(t)$ packet success rate, $\Delta n_i(t)$ neighbor change rate, and $LCS_i(t)$ localization reliability.

- **Action Space:** Continuous action space $\mathcal{A} \in [-1, 1]$ represents HELLO interval adjustments and the Actor network $\mu(\cdot)$ generates

$$a_t = \mu(\mathbf{s}_t|\theta^{\mu}) + \mathcal{N}_t. \tag{21}$$

with the range constraint

$$\Delta T_{\text{HELLO}}(t+1) = \text{Clip}\left(T(t) + a_t,\ T_{\min},\ T_{\max}\right). \tag{22}$$

- **Reward Function:** The system reward is represented by multi-objective evaluation integrating communication and localization:

$$r_t = -w_1 \frac{1}{T(t)} - w_2 \rho_c(t) + w_3 \frac{v_i(t)}{v_{\max}} \cdot \mathbb{E}[\Delta n_i(t)] + w_4 LCS_i(t). \tag{23}$$

The structure of the proposed DDPG-based adaptive HELLO interval algorithm is shown in Fig. 3. During adaptive HELLO interval adjustment, the UAV first observes the current network state s_t, generates an action a_t via the policy network to adjust the HELLO message interval, and subsequently receives the immediate reward r_t and the next state s_{t+1}. The transition (s_t, a_t, r_t, s_{t+1}) is stored into the replay buffer. During training, the algorithm randomly samples mini-batches from the buffer and performs the following updates sequentially: the Critic network optimizes the value function estimation by minimizing the temporal difference error; the Actor network updates its parameters using deterministic policy gradients to maximize the long-term reward; finally, a soft update mechanism is applied to gradually synchronize the target network parameters, ensuring training stability.

IV. Evaluations

We conducts performance validation based on an NS-3/NS3-Gym/GTSAM co-simulation platform. The experimen-

tal scenario is configured in a three-dimensional airspace with dimensions $1000\times1000\times500$ m^3, where GNSS-denied regions are defined as $\{(x, y, z)|x \in [50, 950]\,\text{m}, y \in [50, 950]\,\text{m}, z \in [0, 500]\,\text{m}\}$. UAV nodes are initially deployed by uniform random distribution and their mobility patterns are simulated through a Markovian random walk model. The number of UAVs is varied between 60 and 180, with average flight velocities ranging from 5 to 25 m/s. We compare five approaches to verify the key performance:

- **GPSR routing protocol:** Shorter Euclidean distances are prioritized for greedy next-hop selection.
- **BLPR routing protocol:** Dynamic node characteristics (velocity, distance, trajectory angle) are integrated for predictive forwarding.
- **FFLA localization algorithm:** Pose rectification and UKF-based localization are combined for nonlinear state tracking in GNSS-denied regions.
- **WFGA localization algorithm:** Reliable neighbors are selected via credibility metrics and least-squares optimization are utilized for distributed factor graph localization.
- **CL2F algorithm:** the proposed close-loop communication-localization framework.

As shown in Fig. 4(a), the *Packet Arrival Rate (PDR)* of BLPR and the CL2F-integrated protocol first increases and then decreases with UAV density, while GPSR continuously declines. Both protocols use multi-dimensional optimization incorporating geometric and stability metrics. Their performance improves with node density, with CL2F achieving about 4% higher PDR than BLPR due to adaptive HELLO intervals. However, excessive density causes severe interference, leading to performance degradation in all protocols.

Fig. 4(b) illustrates the relationship between average UAV speed and PDR. The PDR of all three protocols decreases significantly due to rapid topological changes caused by high mobility. The CL2F-integrated routing protocol outperforms GPSR by incorporating a stability-aware neighbor selection mechanism. Compared to BLPR, which evaluates link quality based on the ratio of node distance to maximum speed, CL2F employs a more comprehensive utility function for neighbor assessment. Moreover, CL2F integrates a DDPG-based adaptive HELLO interval mechanism, enabling timely topology updates under high mobility. Therefore, its PDR improves by approximately 5% over BLPR in high-speed scenarios.

Fig. 4(c) shows the trend of *Mean Absolute Error (MAE)* with varying numbers of UAVs. The localization error of all three algorithms first decreases and then increases, due to insufficient position information at low density and increased network interference at high density. Among them, FFLA performs worst, WFGA is relatively stable, while the CL2F-integrated framework demonstrates stronger adaptability in large-scale scenarios by adaptively adjusting HELLO intervals based on network conditions, achieving approximately 22% improvement in MAE over WFGA.

Fig. 4(d) shows when the average speed increases, the MAE of all three algorithms rises due to reduced timeliness of position information and increased error accumulation from rapid topology changes. Among them, FFLA exhibits the most significant performance degradation under high mobility, while CL2F maintains global consistency through its factor graph method in low-speed scenarios, performing comparably to FFLA. Notably, in high-speed environments, CL2F demonstrates superior adaptability thanks to its algorithm-switching mechanism, achieving approximately 14% improvement in MAE over WFGA.

V. Conclusions

A CL2F framework is proposed to iteratively quantify localization reliability and dynamically adjust communication strategies for high-mobility UAV swarm networks in partial GNSS-denied environments. The evaluations confirm CL2F's robustness in maintaining connectivity and precise positioning under dynamic topology disruptions and signal interference.

References

[1] H. Hong, Y. Zhang, and Y. Xie, "Energy-limited uav visiting planning for age-aware wireless-powered sensor networks," in *2023 IEEE 98th Vehicular Technology Conference (VTC2023-Fall)*, 2023, pp. 1–6.

[2] P. Cao, L. Lei, S. Cai, G. Shen, X. Liu, X. Wang, L. Zhang, L. Zhou, and M. Guizani, "Computational intelligence algorithms for uav swarm networking and collaboration: A comprehensive survey and future directions," *IEEE Communications Surveys & Tutorials*, vol. 26, no. 4, pp. 2684–2728, 2024.

[3] N. Bartolini, G. Masi, M. Prata, and F. Trombetti, "Patrolling heterogeneous targets with fanets," in *IEEE INFOCOM 2024 - IEEE Conference on Computer Communications Workshops (INFOCOM WKSHPS)*, 2024, pp. 1–6.

[4] Y. Zhang, Y. Xie, L. Wang, M. Liwang, and X. Wang, "Reconfigurable intelligent surface enhanced wireless localization: Phase optimization for malicious interference mitigation," *IEEE Transactions on Communications*, pp. 1–1, 2025.

[5] M. Y. Arafat and S. Moh, "A q-learning-based topology-aware routing protocol for flying ad hoc networks," *IEEE Internet of Things Journal*, vol. 9, no. 3, pp. 1985–2000, 2022.

[6] Y. Cui, H. Tian, C. Chen, W. Ni, H. Wu, and G. Nie, "New geographical routing protocol for three-dimensional flying ad-hoc network based on new effective transmission range," *IEEE Transactions on Vehicular Technology*, vol. 72, no. 12, pp. 16 135–16 147, 2023.

[7] H. Oliveira, S. S. Dias, and M. G. S. Bruno, "Gnss-denied joint cooperative terrain navigation and target tracking using factor graph geometric average fusion," *IEEE Transactions on Aerospace and Electronic Systems*, vol. 60, no. 1, pp. 991–1005, 2024.

[8] X. Zhu, J. Lai, B. Zhou, P. Lv, and S. Chen, "Weight factor graph co-location method for uav formation based on navigation performance evaluation," *IEEE Sensors Journal*, vol. 23, no. 12, pp. 13 037–13 051, 2023.

[9] C.-H. Ko and S.-H. Wu, "A framework for proactive indoor positioning in densely deployed wifi networks," *IEEE Transactions on Mobile Computing*, vol. 21, no. 1, pp. 1–15, 2022.

[10] H. D. Tuan, A. A. Nasir, A. V. Savkin, H. V. Poor, and E. Dutkiewicz, "Mpc-based uav navigation for simultaneous solar-energy harvesting and two-way communications," *IEEE Journal on Selected Areas in Communications*, vol. 39, no. 11, pp. 3459–3474, 2021.

[11] Y. Zhao, Z. Li, N. Cheng, B. Hao, and X. Shen, "Joint uav position and power optimization for accurate regional localization in space-air integrated localization network," *IEEE Internet of Things Journal*, vol. 8, no. 6, pp. 4841–4854, 2021.